

DINO-SD: Champion Solution for ICRA 2024 RoboDepth Challenge

Yifan Mao* Ming Li* Jian Liu* Jiayang Liu Zihan Qin Chunxi Chu
 Jialei Xu WenBo Zhao Junjun Jiang Xianming Liu[†]
 Harbin Institute of Technology

Abstract

Surround-view depth estimation is a crucial task aims to acquire the depth maps of the surrounding views. It has many applications in real world scenarios such as autonomous driving, AR/VR and 3D reconstruction, etc. However, given that most of the data in the autonomous driving dataset is collected in daytime scenarios, this leads to poor depth model performance in the face of out-of-distribution(OoD) data. While some works try to improve the robustness of depth model under OoD data, these methods either require additional training data or lack generalizability. In this report, we introduce the DINO-SD, a novel surround-view depth estimation model. Our DINO-SD does not need additional data and has strong robustness. Our DINO-SD get the best performance in the track4 of ICRA 2024 RoboDepth Challenge.

1. Overview

Depth estimation, which aims to estimate the distance of every point in the image, is a crucial task in 3D vision with important applications such as autonomous driving[12], augmented reality[22], virtual reality[6], and 3D reconstruction[20]. Compared to acquiring depth using depth sensors such as LiDAR, estimating depth from images can effectively reduce hardware costs and produce dense depth map. This makes depth estimation algorithms the primary choice in these fields.

Depth estimation tasks can be categorized into monocular depth estimation and multi-view depth estimation according to the number of cameras used. Monocular depth estimation is inherently limited by its reliance on a single viewpoint, which compromises its robustness. In contrast, multi-view depth estimation provides a comprehensive 360° view of the surroundings, which is able to more accurate estimation of depth and robust to changes in scene geometry. As sensor technologies advance and manufacturing costs decrease, multi-view depth estimation has progressively replaced monocular depth estimation as the industry

standard. Notable works in this field include MVSNet[21], SurroundDepth[18] and S3Depth[4].

However, existing multi-view depth estimation methods still do not perform satisfactorily in real-world scenarios. The main reason is that real-world sensor data often contains corruptions, such as adverse weather and sensor noise, and most autonomous driving training datasets primarily consist of clean data. Existing methods [4, 18] lack robustness to noise. Several studies have focused on enhancing the robustness of depth estimation[2, 3, 9, 14] through the use of additional training data in different scenes. However, the introduction of additional data still cannot cover all situations in real-world scenarios. Given the prohibitive cost of acquiring large volumes of corrupted data, and considering that expanding training datasets may not encompass all real-world corruptions, developing a robust multi-view depth estimation model capable of performing well on out-of-distribution (OoD) data is imperative.

Inspiration from the Depth Anything[19] framework, we introduce DINO-SD, a novel approach aimed at improving the robustness of surround-view depth estimation models. This framework is designed to handle a variety of environmental conditions and sensor imperfections, enhancing the reliability of depth estimation in autonomous driving and other critical applications.

2. Related Work

2.1. Multi-view Depth Estimation

Multi-view depth estimation aims at estimating the depth of the scene using multi-view information. It can be categorized into stereo matching, multi-view stereo and surround-view depth estimation.

Stereo matching utilizes the left and right camera images to predict the depth. The stereo matching algorithm recovers the depth information of the scene through the basic principles of multi-view geometry. Multi-view stereo matching improves depth estimation model performance by computing the differentiable cost volume of multiple viewpoints and implementing feature fusion to aggregate feature information from multiple viewpoints. MVSNet[21] is the first work

*Equal contribution.

[†]Corresponding author.

to use multiple viewpoints cost volume to estimate the scene depth. Surround-view depth estimation is also a kind of multi-view depth estimation which takes 360° surrounding views as input. SurroundDepth[18] first uses self-attention to process surrounding view images and get the depth maps of surrounding views. S3Depth[4] changes the self attention to adjacent-view cross attention and achieves better performance.

2.2. Robust Depth Estimation

Although depth estimation model performance is greatly improved in daytime scenes, it suffers severely when confronted with OoD data. Some works have explored robust depth estimation, and these can be divided into two categories: data-driven robust depth estimation and model-driven robust depth estimation.

Model-driven robust depth estimation achieves robust depth estimation by introducing new modules or modifying depth model architecture. DeFeat-Net[15] proposes a unified framework aims at improving depth model performance under darkness. RNW[17] uses image enhancement technique and adversarial training to enhance model performance under darkness. WSGD[16] estimates the flow maps and models light changes between adjacent frames to enhance model performance under darkness. The problem with model-driven robust depth estimation is that it is poorly migratable and can only be adapted to a single adverse scene, not to multiple OoD data.

Data-driven robust depth estimation achieves robust depth estimation by introducing other modalities into model training or using the domain adaption to scale up the training dataset. DEISR[7] uses sparse Radar data to enable depth estimation under adverse conditions. R4Dyn[2] uses sparse radar data as weak supervision during training. DET[13] uses thermal images to estimate depth. ADDS[8] uses different encoders to extract invariant and private features of different domains. ITDFA[23] utilizes CycleGAN[24] to translate images into other domains and uses domain adaption method to improve the model robustness. Md4all[3] achieves robust depth estimation by not distinguishing images in standard and challenging conditions, and training the model using knowledge distillation. The problem with methods using other modalities is that the high cost of data collection equipment and manual data labeling limits the development of these methods. The problem with domain adaption is that it needs a translation model to convert normal distribution data into OoD data which requires training translation model and generate training data.

Current robust depth estimation methods lack a generalized model architecture that can be adapted to a wide range of out-of-distribution data, and also rely on additional modal data or artificial data training. How to achieve robust depth estimation without using out-of-distribution data or addi-

tional modal training is a question worth exploring.

3. Technical Approach

3.1. Overview

Given 6 surrounding views $I_s \in \mathbb{R}^{6 \times 3 \times H \times W}$. The goal of the proposed DINO-SD is to output 6 corresponding depth maps $D_s \in \mathbb{R}^{6 \times 1 \times H \times W}$. As shown in Fig. 1, the proposed DINO-SD encompasses three principal phases: feature extracting, fuse and decoding, depth estimation. In the following, we will introduce the three phases in details.

3.2. DINO-SD

Our DINO-SD uses the pretrained DINOv2[10] as encoder, and M-DPT and DPT [11] as decoders. The reason we use Dinov2 is that Dinov2 can extract robust image features compared with other encoders. It helps to improve the model performance when processing the OoD data.

Furthermore, we choose DPT[11] as our decoder. We also modify the structure of DPT to adapt for surround-view depth estimation and propose the Multiview-DPT (M-DPT) as shown in figure 1. We introduce the adjacent-view attention into DPT.

In previous surround-view depth estimation task, SurroundDepth[18] uses cross-view self attention while S3Depth[4] uses adjacent-view cross attention.

Let $F_i \in \mathbb{R}^{N \times C \times \frac{H}{n} \times \frac{W}{n}}$, $i = 1, 2, 3, 4, 5, 6$ be the feature maps obtained from i -th view, where H and W indicate the height and width of the input images, N represents the batchsize, and C stands for the dimensions of the feature map. For self attention, the feature maps F_i are concated and reshaped into $F \in \mathbb{R}^{N \times \frac{6HW}{n^2} \times C}$ and then used to compute the Q, K, V from F . The formular 1 shows the calculation process.

$$\begin{aligned} Q &= W_Q F \\ K &= W_K F \\ V &= W_V F \end{aligned} \tag{1}$$

$$F = \text{softmax}\left(\frac{Q^T K}{\sqrt{C}}\right)V$$

For adjacent-view cross attention, K and V are computed from the adjacent-view feature maps $F_j, j \in (i - 1, i + 1)$. The feature maps F_i are shaped into $F_i \in \mathbb{R}^{N \times \frac{HW}{n^2} \times C}$ and then used to computed the Q, K , and V . The formular 2 shows the calculation process.

$$\begin{aligned} Q &= W_Q F_i \\ K &= W_K F_j \\ V &= W_V F_j \end{aligned} \tag{2}$$

$$F_i = \text{softmax}\left(\frac{Q^T K}{\sqrt{C}}\right)V$$

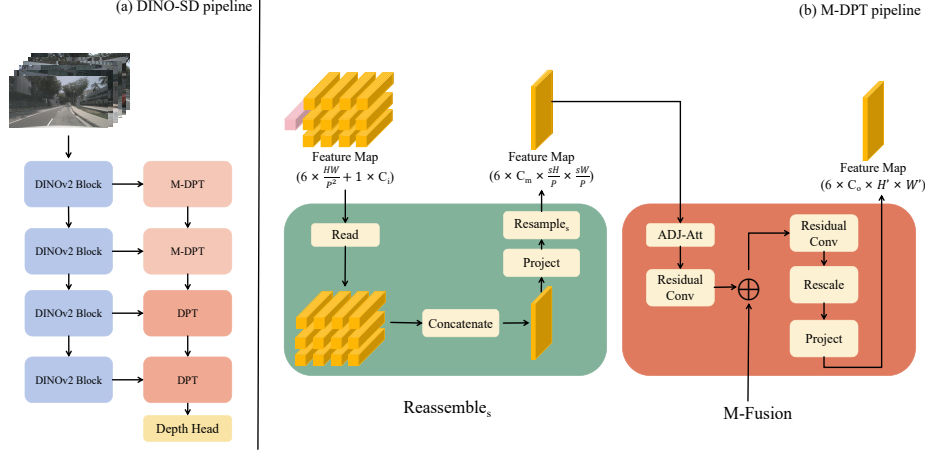


Figure 1. **Our DINO-SD model:** Our DINO-SD model use the pretrained DINOv2 as encoder, M-DPT and DPT as decoder.

S3Depth’s performance is better than SurroundDepth, so we use the adjacent-view cross attention. We also try the cross-view self attention but the results show that adjacent-view cross attention is better than cross-view self attention. More details can be found in section 4. To introduce self attention or cross attention into DPT, we perform the self attention or cross attention operation before the feature maps are fed into the Fusion module of DPT. More details for DPT structure can be found in [11].

Our depth head is very simple, containing only two convolutional layers and a sigmoid head.

3.3. Training Pipeline

Our model training pipeline is shown in the figure 2a. For surrounding-view images $I_s \in \mathbb{R}^{6 \times 3 \times H \times W}$, we first use DINOv2 to extract the feature maps $F \in \mathbb{R}^{6 \times \frac{HW}{p^2} \times C}$ and then we use M-DPT and DPT to decode the feature maps. Finally, we use a depth head to get the depth map $D \in \mathbb{R}^{6 \times 1 \times H \times W}$. We use the LiDAR ground truth to provide the supervision for depth map. We adopt the silog loss to depth supervision:

$$L_{silog} = \frac{1}{n} \sum_i d_i^2 - \frac{\lambda}{n^2} \left(\sum_i d_i \right)^2, \quad (3)$$

where $d_i = \log y_i - \log y_i^*$, y_i represents the predicted depth of i -th pixel and y_i^* represents the ground truth depth of i -th pixel. We set $\lambda = 0.85$.

Furthermore, we use the AugMix loss to make the model be capable to process OoD data. AugMix data augmentation method[5] which mixes the augmented images. We first use AugMix to process the surrounding-view images I_s and get the augmented images I_a . Then, we use our DINO-SD to estimate the depth maps D_a of the augmented images I_a , and use the AugMix loss to make D_s and D_a have similar

distributions. In our experiments, we perform two separate AugMix operations on I_s to obtain D_{a1} and D_{a2} , and calculate the difference between the D_s , D_{a1} , D_{a2} distributions by JS divergence:

$$D_{mix} = \frac{1}{3} (D_s + D_{a1} + D_{a2}),$$

$$L_{AugMix} = \frac{1}{3} (KL(D_s || D_{mix}) + KL(D_{a1} || D_{mix}) + KL(D_{a2} || D_{mix})), \quad (4)$$

where D_{mix} represents the mixed depth map and KL represents the KL divergence.

We also use the smooth loss to maintain the depth map consistency:

$$L_{smooth} = \sum_i |\partial_x d_i^*| e^{-|\partial_x I_i|} + |\partial_y d_i^*| e^{-|\partial_y I_i|}, \quad (5)$$

where $d_i^* = d_i / \bar{d}_i$.

Our loss is the combination of silog loss, augmix loss and smooth loss:

$$L = L_{silog} + \alpha L_{smooth} + \beta L_{AugMix}, \quad (6)$$

we set $\alpha = 10^{-3}$ and $\beta = 10^{-2}$.

3.4. Testing Pipeline

Our testing pipeline is shown in figure 2b. For surrounding-view OoD images, we perform image denoise and equalize operations on the OoD images and then input into our trained DINO-SD. We adopt donoho *et al.* image denoise method[1]. We did not use model ensemble methods to improve the performance of our method.

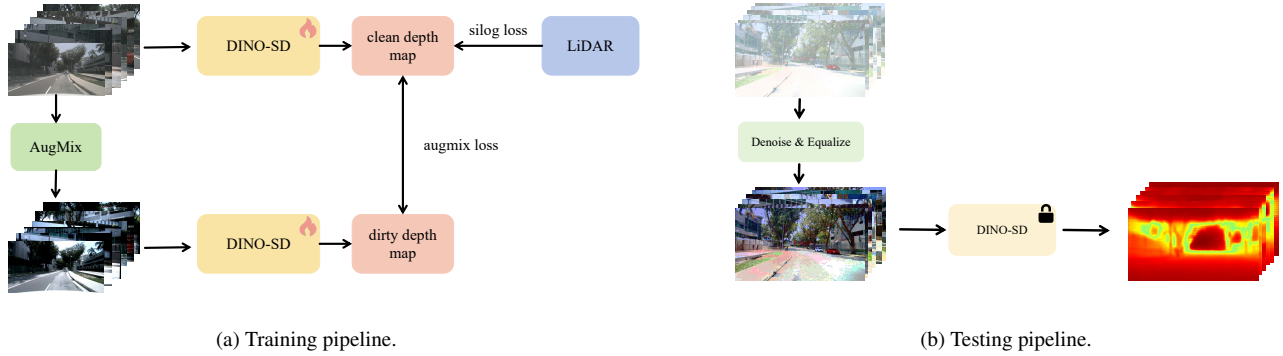


Figure 2. Our training and testing pipeline.

Table 1. Ablation results of DinoSurDepth on the RoboDrive competition leaderboard. The symbol \times indicates that the module was not used, the symbol \checkmark indicates that the module was used, and the best results are highlighted in **bold**.

Method	attention	denoise	equalize	Abs Rel \downarrow	Sq Rel \downarrow	RMSE \downarrow	log RMSE \downarrow	$a1 \uparrow$	$a2 \uparrow$	$a3 \uparrow$
SurroundDepth(Baseline)	self attention	\times	\times	0.3039	3.0596	8.5285	0.4003	0.5439	0.7839	0.8911
DINO-SD	\times	\times	\times	0.2654	2.5803	8.2702	0.3738	0.5873	0.8220	0.9128
DINO-SD	self attention	\times	\times	0.2162	1.9451	7.6721	0.3289	0.6702	0.8512	0.9279
DINO-SD	self attention	\checkmark	\times	0.2074	1.8087	7.4020	0.3145	0.6887	0.8588	0.9340
DINO-SD	self attention	\times	\checkmark	0.2078	1.7107	7.0786	0.3091	0.6844	0.8611	0.9370
DINO-SD	self attention	\checkmark	\checkmark	0.2052	1.7246	7.1974	0.3075	0.6900	0.8651	0.9395
DINO-SD	adjacent-view cross attention	\checkmark	\checkmark	0.1870	1.4683	6.2365	0.2760	0.7339	0.8952	0.9531

4. Experiments

Implementation Details The DINO-SD framework is implemented using PyTorch. It utilizes four NVIDIA GTX 3090 GPUs for model training, each configured as a batch size of 1x6 (for six views). On the leaderboard, our method secured first place across all six metrics. We use the DINOv2 [10] as the backbone, which is pretrained on a massive dataset named LVD-142M, comprising 142 million images. This dataset is assembled from ImageNet-22k, the training split of ImageNet-1k, Google Landmarks, and several fine-grained datasets. In the DINO-SD model, we use the last four blocks of the DINOv2 encoder to extract image features, the M-DPT and DPT to decode feature maps. For the third-to-last and fourth-to-last blocks, we processed the features using M-DPT, with the resample scale set to 1 and 0.5 respectively. For the penultimate and penultimate blocks, we processed the features using DPT with the resample scale set to 2 and 4, respectively. The learning rate for the encoder is $5e-6$ and the learning rate for the decoder is $2e-5$. We employed the CosineAnnealingWarmRestarts method for our model’s optimizer. This scheduler adjusts the learning rate following a cosine annealing pattern, periodically resetting to enhance convergence. We spent 18 hours training for 5 epochs, but ultimately found that the weights from the first epoch achieved the best results on the test set (corrupted images). We believe this was mainly due to the following reasons: Firstly, our batch size was relatively large (4 GPUs \times 6 views), which

led to the model converging quickly; Secondly, there was a significant distribution shift between the corrupted images and clean images, and learning too much from the clean images easily led to overfitting.

Comparative Study The benchmark uses the original depth of the corruption images as ground truth for evaluation purposes. Corruptions are simulated through algorithms encompassing 18 types of corruptions, namely: darkness, brightness, defocus blur, contrast, JPEG compression, impulse noise, motion blur, snow, zoom blur, frost, pixelation, color, quantization, elastic transformation, Gaussian noise, fog, ISO noise, shot noise, and glass blur. Table 2 compares the model’s performance with that of other teams on the RoboDrive competition leaderboard.

Table 2. Quantitative results on the Robodrive competition(Track 4). The **best** scores of each metric are highlighted in **bold**.

Team	Abs Rel \downarrow	Sq Rel \downarrow	RMSE \downarrow	log RMSE \downarrow	$a1 \uparrow$	$a2 \uparrow$	$a3 \uparrow$
HIT-AIIA ¹	0.187	1.468	6.236	0.276	0.734	0.895	0.953
twolones ²	0.211	1.655	6.327	0.294	0.686	0.880	0.946
CUSTZS ³	0.264	2.320	7.961	0.363	0.578	0.816	0.913

Ablation Study In Table 1, we assess the impact of various repair algorithms, decoders, and backbones. The results demonstrate that all configurations yield improvements in the depth estimation task.

The first line is the official baseline SurroundDepth. We

first try DINOv2 as encoder and DPT as decoder. The second line shows that although our DINO-SD do not use any attention mechanism, our DINO-SD performance is better than baseline. In line 3, we try to introduce self attention into DPT and the model performance improved a lot. In lines 4-6, we explore the impact of image denoise and equalization on the results. The results show that both image denoise and equalization help to improve the performance of the model, and the improvement effect is greater when used together. In line 7, we change the self attention into adjacent view cross attention and the results show that the adjacent-view cross attention is better than self attention. The reason adjacent-view cross attention performance better than self attention has explained in S3Depth[4], the adjacent views can offer direct environment information compared with non-adjacent views.

5. Summary

In this work, we propose the DINO-SD, a novel framework that focuses on improving the robustness of the surround-view depth estimation model. We add attention mechanism into DPT and improved the performance of model. The results show that the proposed method is able to handle various corruptions.

References

- [1] David L Donoho and Iain M Johnstone. Ideal spatial adaptation by wavelet shrinkage. *biometrika*, 81(3):425–455, 1994. [3](#)
- [2] Stefano Gasperini, Patrick Koch, Vinzenz Dallabetta, Nassir Navab, Benjamin Busam, and Federico Tombari. R4dyn: Exploring radar for self-supervised monocular depth estimation of dynamic scenes. In *2021 International Conference on 3D Vision (3DV)*, pages 751–760. IEEE, 2021. [1](#), [2](#)
- [3] Stefano Gasperini, Nils Morbitzer, HyunJun Jung, Nassir Navab, and Federico Tombari. Robust monocular depth estimation under challenging conditions. In *Proceedings of the IEEE/CVF international conference on computer vision*, pages 8177–8186, 2023. [1](#), [2](#)
- [4] Xianda Guo, Wenjie Yuan, Yunpeng Zhang, Tian Yang, Chenming Zhang, Zheng Zhu, and Long Chen. A simple baseline for supervised surround-view depth estimation. *arXiv preprint arXiv:2303.07759*, 2023. [1](#), [2](#), [5](#)
- [5] Dan Hendrycks, Norman Mu, Ekin D. Cubuk, Barret Zoph, Justin Gilmer, and Balaji Lakshminarayanan. AugMix: A simple data processing method to improve robustness and uncertainty. *Proceedings of the International Conference on Learning Representations (ICLR)*, 2020. [3](#)
- [6] Yuyan Li, Zhixin Yan, Ye Duan, and Liu Ren. Panodepth: A two-stage approach for monocular omnidirectional depth estimation. In *2021 International Conference on 3D Vision (3DV)*, pages 648–658. IEEE, 2021. [1](#)
- [7] Juan-Ting Lin, Dengxin Dai, and Luc Van Gool. Depth estimation from monocular images and sparse radar data. In *2020 IEEE/RSJ International Conference on Intelligent Robots and Systems (IROS)*, pages 10233–10240. IEEE, 2020. [2](#)
- [8] Lina Liu, Xibin Song, Mengmeng Wang, Yong Liu, and Liangjun Zhang. Self-supervised monocular depth estimation for all day images using domain separation. In *Proceedings of the IEEE/CVF international conference on computer vision*, pages 12737–12746, 2021. [2](#)
- [9] Yifan Mao, Jian Liu, and Xianming Liu. Stealing stable diffusion prior for robust monocular depth estimation. *arXiv preprint arXiv:2403.05056*, 2024. [1](#)
- [10] Maxime Oquab, Timothée Darcet, Theo Moutakanni, Huy V. Vo, Marc Szafraniec, Vasil Khalidov, Pierre Fernandez, Daniel Haziza, Francisco Massa, Alaaeldin El-Nouby, Russell Howes, Po-Yao Huang, Hu Xu, Vasu Sharma, Shang-Wen Li, Wojciech Galuba, Mike Rabbat, Mido Assran, Nicolas Ballas, Gabriel Synnaeve, Ishan Misra, Herve Jegou, Julien Mairal, Patrick Labatut, Armand Joulin, and Piotr Bojanowski. DINOv2: Learning robust visual features without supervision, 2023. [2](#), [4](#)
- [11] René Ranftl, Alexey Bochkovskiy, and Vladlen Koltun. Vision transformers for dense prediction. In *Proceedings of the IEEE/CVF international conference on computer vision*, pages 12179–12188, 2021. [2](#), [3](#)
- [12] Markus Schön, Michael Buchholz, and Klaus Dietmayer. Mgnet: Monocular geometric scene understanding for autonomous driving. In *Proceedings of the IEEE/CVF International Conference on Computer Vision*, pages 15804–15815, 2021. [1](#)
- [13] Ukcheol Shin, Jinsun Park, and In So Kweon. Deep depth estimation from thermal image. In *Proceedings of the IEEE/CVF Conference on Computer Vision and Pattern Recognition*, pages 1043–1053, 2023. [2](#)
- [14] Ukcheol Shin, Jinsun Park, and In So Kweon. Deep depth estimation from thermal image. In *Proceedings of the IEEE/CVF Conference on Computer Vision and Pattern Recognition (CVPR)*, pages 1043–1053, 2023. [1](#)
- [15] Jaime Spencer, Richard Bowden, and Simon Hadfield. Defeatnet: General monocular depth via simultaneous unsupervised representation learning. In *Proceedings of the IEEE Conference on Computer Vision and Pattern Recognition*, 2020. [2](#)
- [16] Madhu Vankadari, Stuart Golodetz, Sourav Garg, Sangyun Shin, Andrew Markham, and Niki Trigoni. When the sun goes down: Repairing photometric losses for all-day depth estimation. In *Proceedings of The 6th Conference on Robot Learning*, pages 1992–2003. PMLR, 2023. [2](#)
- [17] Kun Wang, Zhenyu Zhang, Zhiqiang Yan, Xiang Li, Baobei Xu, Jun Li, and Jian Yang. Regularizing nighttime weirdness: Efficient self-supervised monocular depth estimation in the dark. In *Proceedings of the IEEE/CVF International Conference on Computer Vision (ICCV)*, pages 16055–16064, 2021. [2](#)
- [18] Yi Wei, Linqing Zhao, Wenzhao Zheng, Zheng Zhu, Yongming Rao, Guan Huang, Jiwen Lu, and Jie Zhou. Surround-depth: Entangling surrounding views for self-supervised multi-camera depth estimation. In *Conference on Robot Learning*, pages 539–549. PMLR, 2023. [1](#), [2](#)
- [19] Lihe Yang, Bingyi Kang, Zilong Huang, Xiaogang Xu, Jiashi Feng, and Hengshuang Zhao. Depth anything: Unleashing the power of large-scale unlabeled data. In *CVPR*, 2024. [1](#)
- [20] Xingbin Yang, Liyang Zhou, Hanqing Jiang, Zhongliang Tang, Yuanbo Wang, Hujun Bao, and Guofeng Zhang. Mobile3drecon: Real-time monocular 3d reconstruction on a mobile phone. *IEEE Transactions on Visualization and Computer Graphics*, 26(12):3446–3456, 2020. [1](#)
- [21] Yao Yao, Zixin Luo, Shiwei Li, Tian Fang, and Long Quan. Mvsnet: Depth inference for unstructured multi-view stereo. *European Conference on Computer Vision (ECCV)*, 2018. [1](#)
- [22] Mehmet Kerim Yucel, Valia Dimaridou, Anastasios Drosou, and Albert Saa-Garriga. Real-time monocular depth estimation with sparse supervision on mobile. In *Proceedings of the IEEE/CVF Conference on Computer Vision and Pattern Recognition*, pages 2428–2437, 2021. [1](#)
- [23] Chaoqiang Zhao, Yang Tang, and Qiyu Sun. Unsupervised monocular depth estimation in highly complex environments. *IEEE Transactions on Emerging Topics in Computational Intelligence*, 6(5):1237–1246, 2022. [2](#)
- [24] Jun-Yan Zhu, Taesung Park, Phillip Isola, and Alexei A Efros. Unpaired image-to-image translation using cycle-consistent adversarial networkss. In *Computer Vision (ICCV), 2017 IEEE International Conference on*, 2017. [2](#)